Research Article

Tang Yunchao, Chen Zheng*, Feng Wanhui, Nong Yumei, Li Cong, and Chen Jieming

Combined effects of nano-silica and silica fume on the mechanical behavior of recycled aggregate concrete

https://doi.org/10.1515/ntrev-2021-0058
received June 23, 2021; accepted August 1, 2021

Abstract: Recycled aggregate concrete (RAC) is an environmentally friendly material. However, owing to inherent characteristics of the recycled aggregate (RA), it is difficult to promote and apply it in structural engineering. Silica fume (SF) and nano-silica (NS) have different characteristics as additives for RAC. It has been proven that adding SF only enhances the strength of RAC at a later stage, and NS can improve the early strength of RAC owing to its high pozzolanic activity. In this study, to further improve the properties of RAC, two types of additives were combined into RAC, which was named SF-NS-modified RAC (SSRAC). Compression and split tensile tests were conducted to analyze the mechanical properties of SSRAC at different curing ages. The results indicated that the combined addition of NS and SF improved the performance of RAC at early and later curing ages.

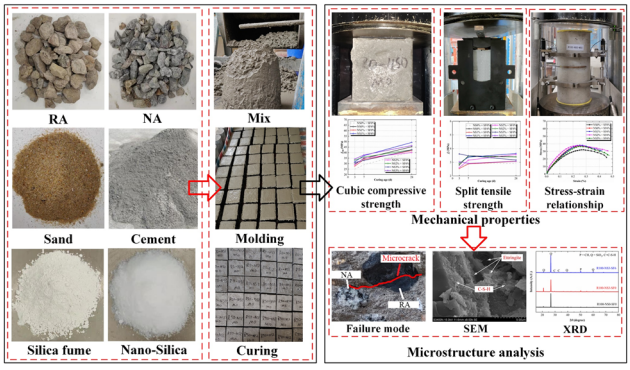

Graphical abstract

Scanning electron microscopy and X-ray diffraction analyses were performed to explore the NS and SF mechanism. The results indicated that SF and NS in SSRAC had a good pozzolanic effect and underwent a secondary hydration reaction with calcium hydroxide to increase the production of calcium silicate hydrate, resulting in an increase in the properties of the interface transition zone. Finally, 6% SF and 2 or 3% NS are recommended as supplementary cementitious materials for RAC.

Keywords: recycled aggregate concrete, nano-silica, silica fume, mechanical behavior, microstructure analysis

1 Introduction

In recent years, with the improvement of comprehensive strength and urbanization speed in China, the number of constructions, and consequently the consumption of concrete, has considerably increased [1–3]. This phenomenon leads to an increase in the demand for natural aggregates (NAs), such as sand and gravel. As NAs are nonrenewable resources, it is urgent to seek new types of aggregates [4,5]. In this regard, construction and demolition (C&D) waste has been considered to be used as aggregate. These C&D wastes can be converted into recycled aggregates (RAs) after a certain procedure [6]. RAs can

* **Corresponding author: Chen Zheng,** Key Laboratory of Disaster Prevention and Structural Safety of China Ministry of Education, School of Civil Engineering and Architecture, Guangxi University, Nanning, 530004, China; Guangxi Key Laboratory of Disaster Prevention and Engineering Safety, Guangxi University, Nanning, 530004, China, e-mail: chenzheng@gxu.edu.cn
Tang Yunchao: Key Laboratory of Disaster Prevention and Structural Safety of China Ministry of Education, School of Civil Engineering and Architecture, Guangxi University, Nanning, 530004, China; Guangxi Key Laboratory of Disaster Prevention and Engineering Safety, Guangxi University, Nanning, 530004, China; College of Urban and Rural Construction, Zhongkai University of Agriculture and Engineering, Guangzhou, Guangdong, 510006, China
Feng Wanhui: College of Urban and Rural Construction, Zhongkai University of Agriculture and Engineering, Guangzhou, Guangdong, 510006, China
Nong Yumei, Li Cong: Key Laboratory of Disaster Prevention and Structural Safety of China Ministry of Education, School of Civil Engineering and Architecture, Guangxi University, Nanning, 530004, China; Guangxi Key Laboratory of Disaster Prevention and Engineering Safety, Guangxi University, Nanning, 530004, China
Chen Jieming: School of Civil and Transportation Engineering, Guangdong University of Technology, Guangzhou, 510000, China

partially replace NAs in the production of concrete, resulting in a green construction material called recycled aggregate concrete (RAC) [7]. The utilization of RA alleviates the shortage of natural resources [8–11]. However, the surface of the RA is covered with old mortar, resulting in a significant effect on the interface transition zone (ITZ) of the RAC. In other words, in addition to the ITZ between the NA and new mortar, there is another ITZ between the new mortar and old mortar on the surface of the RA [12]. Therefore, it is accepted that high RA replacement rate is not recommended in construction engineering. In other words, how to effectively and conveniently improve the mechanical properties of ITZs and old cement mortar at early and later curing ages has become the key to develop high-strength RAC and the wide application of RAC in construction engineering with high RA replacement rate.

Compared with natural aggregate concrete (NAC), RAC has higher porosity and more internal microcracks [13] caused by the recycling process. Therefore, the application rate of RAC is not very high, and the replacement percentage of RA is one of the key factors affecting the mechanical properties of RAC [14]. Therefore, the replacement rate of RA is relatively low (less than 50%) if using RAC in construction engineering. Most of the above research [13,14] focused on the mechanical properties of RAC with different RA replacement ratio and did not further study how to improve the performance of RAC. In other words, if using high RA replacement rate in RAC, some improving methods should be employed.

To improve the properties of RAC, many scholars focus on the treatment method of RAs, such as using physical or chemical activation to improve the performance of RA. Saravanakumar *et al.* [15] pretreated RAs with acids and observed an increase in the compressive strength of the RAC produced. Hosseini Zadeh *et al.* [16] found that CO_2 can react with calcium hydroxide (CH) and calcium silicate hydrate (C–S–H) existing in the old mortar on the surface of RAs, and the new compound product can fill the pores in the mortar, which reduces the porosity and improves the strength of RAC. Khushnood *et al.* [17] modified the surface of RAC by using bacteria to deposit calcium carbonate, which significantly reduced the water absorption and increased the compressive strength.

As the strength of adhered mortar in RAs is usually much lower than that in natural aggregate and new cement paste, porous ITZ may be the weakest zone in RAC, which has a significant impact on the performance of RAC. Therefore, how to improve the properties of ITZs and old cement mortar has become the key to develop high-strength RAC and the wide application of RAC in construction engineering. In addition, the effect of mentioned methods [15–17] of activation or modification of RAs to improve RAC characteristics is limited, because they have some disadvantages, such as complicated procedures or introduce some harmful ions (Cl^-, SO_4^{2-}). Thus, these methods are difficult to be extensively applied in construction engineering.

In contrast, the use of supplementary cementitious materials (SCMs) is a convenient and effective method to improve mechanical properties of concrete. Commonly used SCMs mainly include ground blast furnace slag (GBFS), silica fume (SF), and fly ash (FA) [18,19]; these materials react with CH formed by cement hydration and considerably improve the properties of the ITZ [20]. Among them, the pozzolanic activity of SF is higher than that of FA and GBFS; therefore, lower percentages of SF are required. Miraldo *et al.* [21] indicated that SF can improve the compressive strength of RAC to exceed that of NAC, thus RAC with SF (SFRAC) can be applied to structural engineering. Cakir and Sofyanli [22] indicated that SF mainly participates in the pozzolanic reaction of concrete, but it does not effectively enhance the mechanical properties of concrete at early curing ages. This phenomenon indicates that the effect of SF mainly occurs in the later stages of concrete hardening.

Recently, many scholars have focused on the application of nanomaterials in concrete [23–26]. The use of nanomaterials as particulates in addition to conventional materials increases the mechanical properties of concrete [27]. Nano-silica (NS) [28] is a nano-sized SCM that improves the properties of concrete, further refining the particle size distribution of raw materials and exhibiting a higher pozzolanic activity than SF. The results obtained by Fallah and Nematzadeh [29] and Zareei *et al.* [30] indicated that NS can be an excellent alternative for reducing cement consumption in the production of high-strength concrete. Because of its high specific surface area and high reactivity, NS can promote the hydration of cement, improve the strength of concrete at an early age, and reduce the porosity to form a dense microstructure [31]. Recently, Ying *et al.* [32] used NS to modify RAC (NSRAC), and the results indicated that NS was also suitable for RAC, resulting in an improvement in the RAC microstructure.

Among various types of SCMs, although the enhancement effect of SF on RAC is better than FA and GGFS [18–20], the early-age strength still needs to be improved. Increasing the early-age strength of concrete can improve the engineering efficiency, so as to meet the strength requirements as soon as possible. However, there are few studies on RAC improvement methods that take

into account both early and late ages. Different from SF, because NS has stronger pozzolanic effect than SF, the enhancement effect of NS on RAC is mainly concentrated at the early age, but the growth effect of strength is weak at the later age. In addition, the particle size of NS is much smaller than that of SF; the internal pores of RAC can only be filled by the products of pozzolanic reaction reacted with NS, but not by physical filling together.

According to the characteristics of SF and NS and their effects on the properties of concrete, some researchers have studied the combined use of SF and NS in NAC or cement mortar. Zhang *et al.* [33] studied cement mortars modified with SF and NS. They found that SF and NS consumed a large amount of CH to form a dense C–S–H gel during the hydration of cement and were also important in grading filling in different sizes combined with other SCMs. Bernal *et al.* [34] studied NAC with SF and NS and found that the improvements in workability and strength were different than those obtained when using only NS or SF. Although combined using of NS and SF can effectively improve the mechanical properties of NAC at early and late ages [33,34], the studies about combined using of SF and NS on RAC are still lacking. Because of the different microstructures of NA and RA, it is necessary to further study the mechanical properties of the SF-NS-modified RAC (SSRAC) at different curing ages to validate the feasibility of SSRAC in engineering application.

In this study, considering as test variables replacement percentage of RA (0, 50, and 100%), SF content (0, 3, 6, and 9%), NS content (0, 1, 2, and 3%), and curing age (3, 7, and 28 days), the effects of SF and NS on mechanical properties and microstructural performances of SSRAC are discussed. The purpose of this investigation is to explore the optimal amount of the SCMs analyzed to provide a reference for engineering applications of RAC with high performance.

2 Raw materials and specimen preparations

2.1 Raw materials

SSRAC is composed of cement, fine aggregate, coarse aggregate, SCMs, and tap water. Ordinary Portland cement (P. O. 42.5R), in accordance with the requirements of Chinese standard GB175-2007 [35], was utilized in all mixes. The physical properties and chemical compositions of the cement are listed in Table 1. Continuously graded sand with a fine modulus of 2.62 and a maximum size of 5 mm was used as the fine aggregate, and the grading curve is shown in Figure 1(a). Two types of continuously graded coarse aggregates were used (NA and RA) with particle sizes of 5–31.5 mm, as shown in Figure 1(b). The physical properties of NA and RA are listed in Table 2, according to Chinese standards JGJ52-2006 [36] and GB/T 25177-2010 [37]. SF and NS were used as SCMs and polycarboxylate superplasticizer was used as an admixture. The superplasticizer was the polycarboxylate high-performance water-reducing agent QC-PL2 provided by Qiangli Construction Materials Co., Ltd., with a water-reducing efficiency of 25%. The SF and NS used were both in the form of white powder solids. The physical properties of the NS and SF are summarized in Table 3. Photographs of the SF and NS are shown in Figure 2.

Table 1: Physical properties and chemical composition of cement

Loss on ignition (%)	Blaine-specific surface area (m^2/kg)	Setting time (min)		Flexural strength (MPa)		Compressive strength (MPa)	
		Initial	Final	3 days	28 days	3 days	28 days
3.05	376	150	230	6.2	8.7	30.9	52.7
SO_3 (%)		MgO (%)			Cl^- (%)		
2.32		3.15			0.013		

2.2 Mix proportion

Because RA has high water absorption, and NS has poor dispersion and high water absorption, there are some shortcomings in the preparation process of SSRAC, such as low slump and difficulty in even mixing. In the mix proportion design, the dosage of superplasticizer (1.2, 1.5, 2.5, and 3.5% of binder mass) was mainly determined by the dosage of NS (0, 1, 2, and 3%). With the increase in NS dosage, the dosage of the superplasticizer increased gradually. In addition, because of the high water absorption of RA, additional water was added. The RAs replaced NAs in equal volumes. To explore the effect of SF and NS on the mechanical properties of RAC, SSRAC, SFRAC, and NSRAC were prepared. The mix proportions are listed in Table 4. In the specimen ID, "R" represents the RA replacement rate and "NS" and "SF" represent the NS and SF contents, respectively. Moreover, control groups were set to eliminate the influence of the superplasticizer among the mix proportions analyzed without any NS and SF, where "J" represents the dosage of superplasticizer.

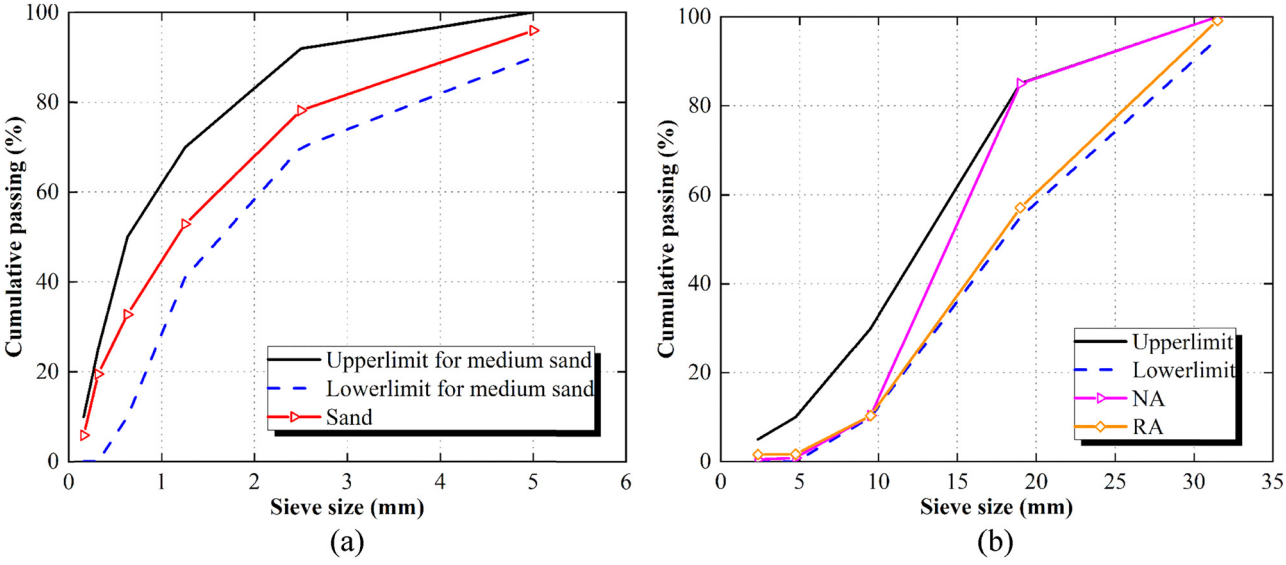

Figure 1: Grading curves of aggregates: (a) fine and (b) coarse aggregates.

Table 2: Physical properties of coarse aggregates

	NA (experiment)	NA (standard)	RA (experiment)	RA (standard)
Apparent density (kg/m^3)	2,765	—	2,484	—
Sediment content (%)	0.22	≤1.0	0.88	≤1.0
Water absorption (%)	0.8	—	2.5	≤3.0
Elongated Particles (%)	8.9	≤15	9.3	≤10
Impurities (%)	0	—	1.0	≤1.0

2.3 Specimens preparation

To produce the SSRAC mixes, coarse aggregate, fine aggregate, and cement were first poured into a concrete mixer and mixed for approximately 120 s. As NS has poor dispersibility and easily agglomerates in water [38], a high-speed stirring rod was used to stir NS in water for 60 s with a superplasticizer. After premixing, this liquid containing NS was added into the concrete mixer, and the mixture was mixed for 150 s. Subsequently, fresh concrete was cast into molds, and the workability was evaluated. The specimens were demolded after 24 h and cured under standard conditions (20 ± 2°C, 95% relative humidity) for the remaining 2, 6, and 27 days (tested at 3, 7, and 28 days, respectively).

Table 3: Physical properties of SF and NS

	Specific surface area (m^2/g)	SiO_2 content (%)	Average particle size
SF	21	98.1	0.1–0.3 μm
NS	230	99.8	7–40 nm

3 Experimental arrangements

3.1 Compression test

According to the Chinese standard GB/T 50081-2019 [39], compression at a loading rate of 0.5 MPa/s was applied to 150-mm cubes, using a universal testing machine (Matest C088-01, Italy) to determine the cubic compressive strength (f_{cu}) of the specimens. Three cubes were tested in each

(a) (b)

Figure 2: Photos of (a) SF and (b) NS.

Table 4: Mix proportions

Series	Specimen ID	Mix proportion (kg/m^3)						
		Cement	SF	NS	Water	RA	NA	Superplasticizer
RAC	R0-NS0-SF0	344	0	0	168	0	1,170	4.13
	R50-NS0-SF0	344	0	0	183	526	585	4.13
	R100-NS0-SF0	344	0	0	198	1,051	0	4.13
SSRAC	R0-NS0-SF6	323.36	20.64	0	168	0	1,170	4.13
	R0-NS1-SF6	319.92	20.64	3.44	168	0	1,170	5.17
	R0-NS2-SF6	316.48	20.64	6.88	168	0	1,170	8.61
	R0-NS3-SF6	313.04	20.64	10.32	168	0	1,170	12.05
	R50-NS0-SF6	323.36	20.64	0	183	526	585	4.13
	R50-NS1-SF6	319.92	20.64	3.44	183	526	585	5.17
	R50-NS2-SF6	316.48	20.64	6.88	183	526	585	8.61
	R50-NS3-SF6	313.04	20.64	10.32	183	526	585	12.05
	R100-NS0-SF6	323.36	20.64	0	198	1,051	0	4.13
	R100-NS1-SF6	319.92	20.64	3.44	198	1,051	0	5.17
	R100-NS2-SF6	316.48	20.64	6.88	198	1,051	0	8.61
	R100-NS3-SF6	313.04	20.64	10.32	198	1,051	0	12.05
NSRAC	R0-NS1-SF0	340.56	0	3.44	168	0	1,170	5.17
	R0-NS2-SF0	337.12	0	6.88	168	0	1,170	8.61
	R0-NS3-SF0	333.68	0	10.32	168	0	1,170	12.05
	R50-NS1-SF0	340.56	0	3.44	183	526	585	5.17
	R50-NS2-SF0	337.12	0	6.88	183	526	585	8.61
	R50-NS3-SF0	333.68	0	10.32	183	526	585	12.05
	R100-NS1-SF0	340.56	0	3.44	198	1,051	0	5.17
	R100-NS2-SF0	337.12	0	6.88	198	1,051	0	8.61
	R100-NS3-SF0	333.68	0	10.32	198	1,051	0	12.05
SFRAC	R0-NS0-SF3	333.68	10.32	0	168	0	1,170	4.13
	R0-NS0-SF6	323.36	20.64	0	168	0	1,170	4.13
	R0-NS0-SF9	313.04	30.96	0	168	0	1,170	4.13
	R50-NS0-SF3	333.68	10.32	0	183	526	585	4.13
	R50-NS0-SF6	323.36	20.64	0	183	526	585	4.13
	R50-NS0-SF9	313.04	30.96	0	183	526	585	4.13
	R100-NS0-SF3	333.68	10.32	0	198	1,051	0	4.13
	R100-NS0-SF6	323.36	20.64	0	198	1,051	0	4.13
	R100-NS0-SF9	313.04	30.96	0	198	1,051	0	4.13
Control group	R100-J0	344	0	0	198	1,051	0	0
	R100-J1.5	344	0	0	198	1,051	0	5.17
	R100-J2.5	344	0	0	198	1,051	0	8.61
	R100-J3.5	344	0	0	198	1,051	0	12.05

group to ensure that the dispersion of data did not exceed 15% (the strength of each specimen was no more than 15% of the intermediate value), and the average value was calculated. A photograph of the cubic compression test is shown in Figure 3.

In addition, based on the ASTM standard C469 [40], four strain gauges were mounted, and two linear variable differential transformers (LVDTs) were set at the mid-sections of Φ150 × 300 mm cylinders to measure the elastic properties (Young's modulus E and Poisson's ratio υ). As shown in Figure 4, four strain gauges, arranged as two diametrically opposite pairs, were used: one pair (10 mm length) for measurement of axial strain and another pair (8 mm length) for circumferential strain. Two LVDTs were employed to capture the axial deformation, particularly for the plastic zone under compression. The loading rate was set to 0.18 mm/min, and all signals were collected by a strain acquisition instrument (JM3841, Yangzhou Jingming Technology Co., Ltd., China). After the specimen reached the ultimate load, the compression stopped when the load decreased to 80% of the ultimate load. The frequency was set to 1 Hz. Three cylinders were tested in each group and the average value was determined.

Figure 3: Photograph of the cubic compression test.

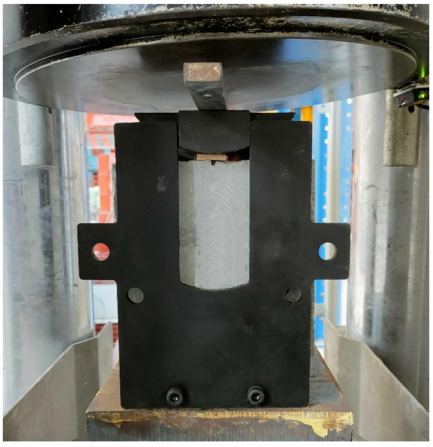

Figure 5: Photograph of the split tensile test.

3.2 Split tensile test

Similarly, the split tensile test was based on the Chinese standard GB 50081-2019 [39], and the customized test fixture was used in the universal testing machine, as shown in Figure 5. Compression at a loading rate of 0.05 MPa/s was applied to 150-mm cubes to determine the split tensile strength (f_t) of the specimens. Three cubes were tested in each group and the average value was determined.

3.3 Microstructure analysis

The surface morphology of the specimens was observed using a scanning electron microscope (SEM, S-3400N, Hitachi, Japan, Figure 6). To improve the conductivity of the samples, they were sprayed with gold in an ion sputtering apparatus. The cement mortar region and ITZ were enlarged and observed [41–43]. In addition, using the X-ray diffractometer (XRD, D8 Advance, Bruker) technique [43–45], the diffraction patterns of the specimens were obtained to analyze the crystal structure.

4 Experimental results

4.1 Effect of superplasticizer

To explore the influence of the polycarboxylate superplasticizer on RAC, the workability and cubic compressive strength of the control group without NS and SF at an early age were tested, and the experimental results are shown in Table 5. Because the hardening of concrete is mainly in the early curing age, only the effect of the superplasticizer content on the early-age strength was explored. On the one hand, the slump of the RAC increased when the dosage of superplasticizer increased. On the other hand, for the ages of 3 and 7 days, the compressive strength of RAC changed slightly (less than 5%) with an increase in the superplasticizer content. It

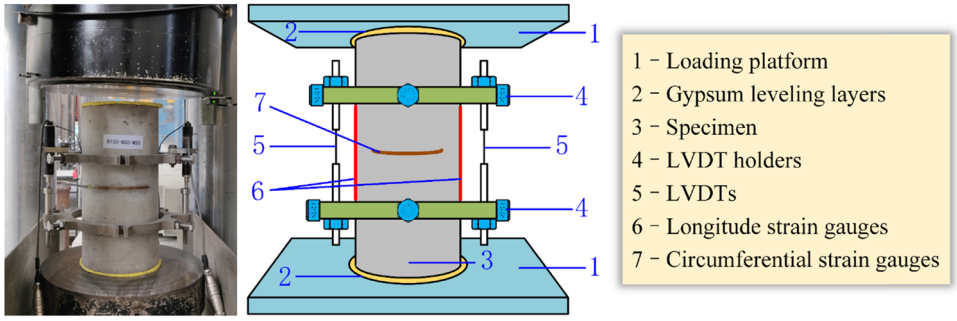

Figure 4: Photograph and sketch of the uniaxial compression test for elastic properties.

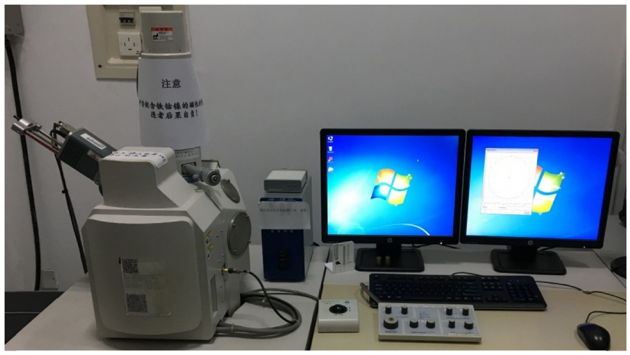

Figure 6: Photograph of the SEM.

can be considered that the superplasticizer had no effect on the compressive strength of RAC at different curing ages. Therefore, the influence of the superplasticizer on the strength of concrete was neglected in the following analysis.

4.2 Experimental results of cubic compressive strength

The experimental results of the workability and cubic compressive strength of RAC, NSRAC, SFRAC, and SSRAC are summarized in Table 6. As shown in Table 5, without any additives, the slump of RAC with 100% RA replacement rate was only 33 mm, and the fluidity was poor. This was due to the high water absorption of RAs; the mixing water was absorbed, resulting in the reduction of free water content in the mixture. Previous studies have also indicated that the addition of NS and SF also reduces the fluidity of concrete [46]. Moreover, the direct addition of NS and SF into RAC also reduces its fluidity, which is extremely disadvantageous to engineering applications of RAC. Based on the mixing procedures in Subsection 2.3, the slump of each group of specimens (Table 6) reached a relatively good value, and the fluidity satisfied the requirements of engineering application and transportation.

Table 5: Workability and compressive strength

Specimen ID	Slump (mm)	f_{cu} (MPa)	
		3 days	7 days
R100-J0	33	27.65	32.94
R100-J1.5	86	28.44	33.98
R100-J2.5	154	25.86	32.23
R100-J3.5	185	26.04	31.63

Table 6: Experimental results of cubic compressive strength

Series	Specimen ID	Slump (mm)	f_{cu} (MPa)		
			3 days	7 days	28 days
RAC	R0-NS0-SF0	155	39.42	48.55	53.72
	R50-NS0-SF0	153	34.48	43.16	49.92
	R100-NS0-SF0	140	24.94	28.98	40.62
NSRAC	R0-NS1-SF0	70	42.89	51.70	57.79
	R0-NS2-SF0	94	44.03	55.81	60.34
	R0-NS3-SF0	121	42.50	52.89	62.19
	R50-NS1-SF0	70	34.06	41.04	44.92
	R50-NS2-SF0	95	36.20	44.33	48.95
	R50-NS3-SF0	107	34.25	44.82	49.86
	R100-NS1-SF0	78	27.78	33.75	41.86
	R100-NS2-SF0	45	28.98	35.18	40.10
	R100-NS3-SF0	65	31.00	32.96	42.54
SFRAC	R0-NS0-SF3	150	39.10	45.71	61.51
	R0-NS0-SF6	210	47.56	51.91	67.47
	R0-NS0-SF9	155	42.92	55.46	67.99
	R50-NS0-SF3	140	31.64	39.84	49.74
	R50-NS0-SF6	188	36.80	44.61	56.46
	R50-NS0-SF9	145	35.24	42.38	54.00
	R100-NS0-SF3	120	22.23	26.61	39.29
	R100-NS0-SF6	165	29.64	34.76	45.40
	R100-NS0-SF9	145	28.01	34.83	43.48
SSRAC	R0-NS1-SF6	145	40.00	51.99	62.58
	R0-NS2-SF6	170	42.93	48.51	59.94
	R0-NS3-SF6	175	46.32	49.65	68.86
	R50-NS1-SF6	168	37.41	41.88	53.98
	R50-NS2-SF6	165	37.21	45.52	54.54
	R50-NS3-SF6	175	37.55	43.11	50.45
	R100-NS1-SF6	150	31.73	37.31	49.32
	R100-NS2-SF6	175	33.21	35.99	42.66
	R100-NS3-SF6	190	34.25	37.92	46.43

4.2.1 Effect of RA replacement percentage

Figure 7 shows the relationship between f_{cu} and RA replacement percentage at various curing ages, where the control group is RAC without SF and NS under different RA replacement percentages. As shown in Figure 7(a), for the three curing ages (3, 7, and 28 days), f_{cu} of NSRAC decreased with an increase in the RA replacement rate. Compared with NSRAC with 0% RA replacement rate, the average decreases of f_{cu} with 50 and 100% RA replacement were 19 and 33% at 3 days (19 and 36% at 7 days and 20 and 31% at 28 days), respectively. Thus, RA replacement is a key factor in the strength of RAC. In contrast, under the same RA replacement ratio, the strength of NSRAC was still higher than that of the control group (RAC) when the NS content was 3%, particularly at 3 and 7 days. Therefore, NS considerably improved the early strength of RAC, but had little effect on the later strength.

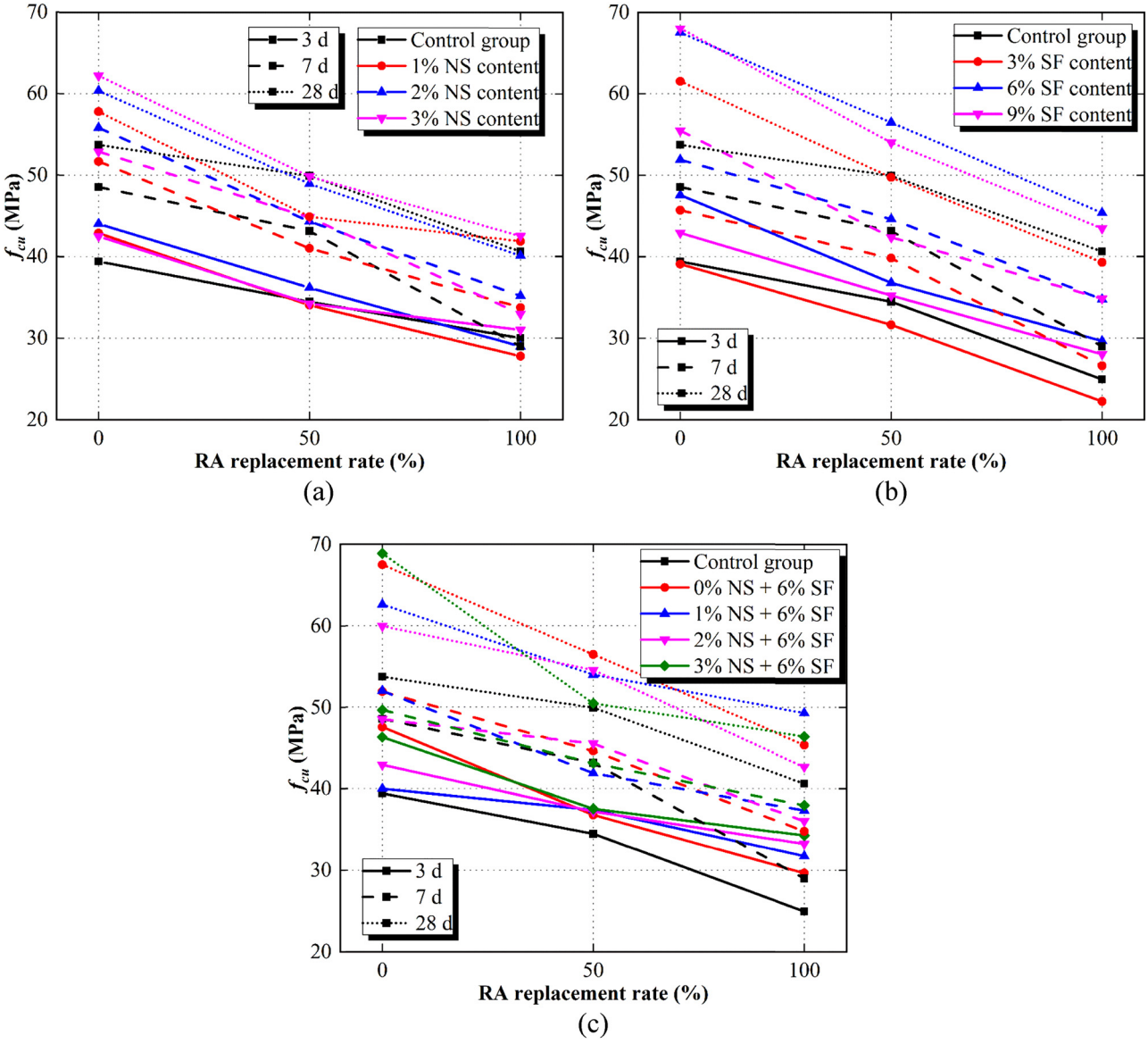

Figure 7: Effect of RA replacement percentages on the cubic compressive strength of (a) NSRAC, (b) SFRAC, and (c) SSRAC.

As shown in Figure 7(b), for the three curing ages (3, 7, and 28 days), f_{cu} of SFRAC decreased with an increase in the RA replacement percentage. Compared with SFRAC with 0% RA replacement, the average decreases of f_{cu} with 50 and 100% RA replacement percentages were 20 and 39% at 3 days (16 and 38% at 7 days and 19 and 35% at 28 days), respectively. In contrast, under the same RA replacement ratio, when the SF content was no less than 6%, the SF clearly increased the strength. The optimal SF content was 6%, and the strength increased by 15, 10, and 16% at 3, 7, and 28 days, respectively. Therefore, a 6% SF content was selected for the following analyses.

As shown in Figure 7(c), for the three curing ages (3, 7, and 28 days), f_{cu} of SSRAC decreased with an increase in the RA replacement percentage. The reductions in f_{cu} of SSRAC with RA replacement were considerably smaller than those of NSRAC and SFRAC. When the RA replacement was 50% (100%), the average decreases of f_{cu} at the three curing ages were smaller by 7% (13%), 5% (11%), and 3% (5%), respectively. This phenomenon indicated that the effect of adding SF and NS on the f_{cu} of RAC was more evident than that of adding SF or NS alone.

The effects of RA replacement percentages on the compressive strength of RAC were consistent with those of some studies [13,47]. With an increase in the RA replacement, the internal microcracks and void ratio also increased, causing the strength of RAC to be lower than that of NAC. Therefore, additives must be added to enhance its properties.

4.2.2 Effect of SCMs contents

Figure 8 depicts the effect of the SCMs contents on the f_{cu} of RAC. As shown in Figure 8(a), when the RA replacement percentage was 0%, NS improved the f_{cu} of RAC at different curing ages. Except for the age of 28 days, the strength increased with the increase in NS content, and for other ages, it reached a peak at 2%. When the RA replacement was 50%, the f_{cu} of RAC decreased with a low NS content (1%). For a RA replacement of 100%, NS enhanced the f_{cu} of RAC at early curing ages, but it had little effect at 28 days. This is because NS mainly promotes the hydration reaction of cement in early curing ages (less than 3 days), thus improving the f_{cu} of RAC. In later stages, NS powders only fill internal pores, and the increase in f_{cu} is not evident.

As shown in Figure 8(b), with an increase in the content of SF, f_{cu} of SFRC at different ages generally showed a tendency of first decreasing, then increasing, and finally decreasing. This means that excessively low or high SF contents affect SFRC properties. There is an optimal SF content to achieve the highest f_{cu}. In this investigation, the SF content of 6% was considered to be optimal.

As shown in Figure 8(c), under the same SF content (6%), when the RA replacement percentages were 0 and

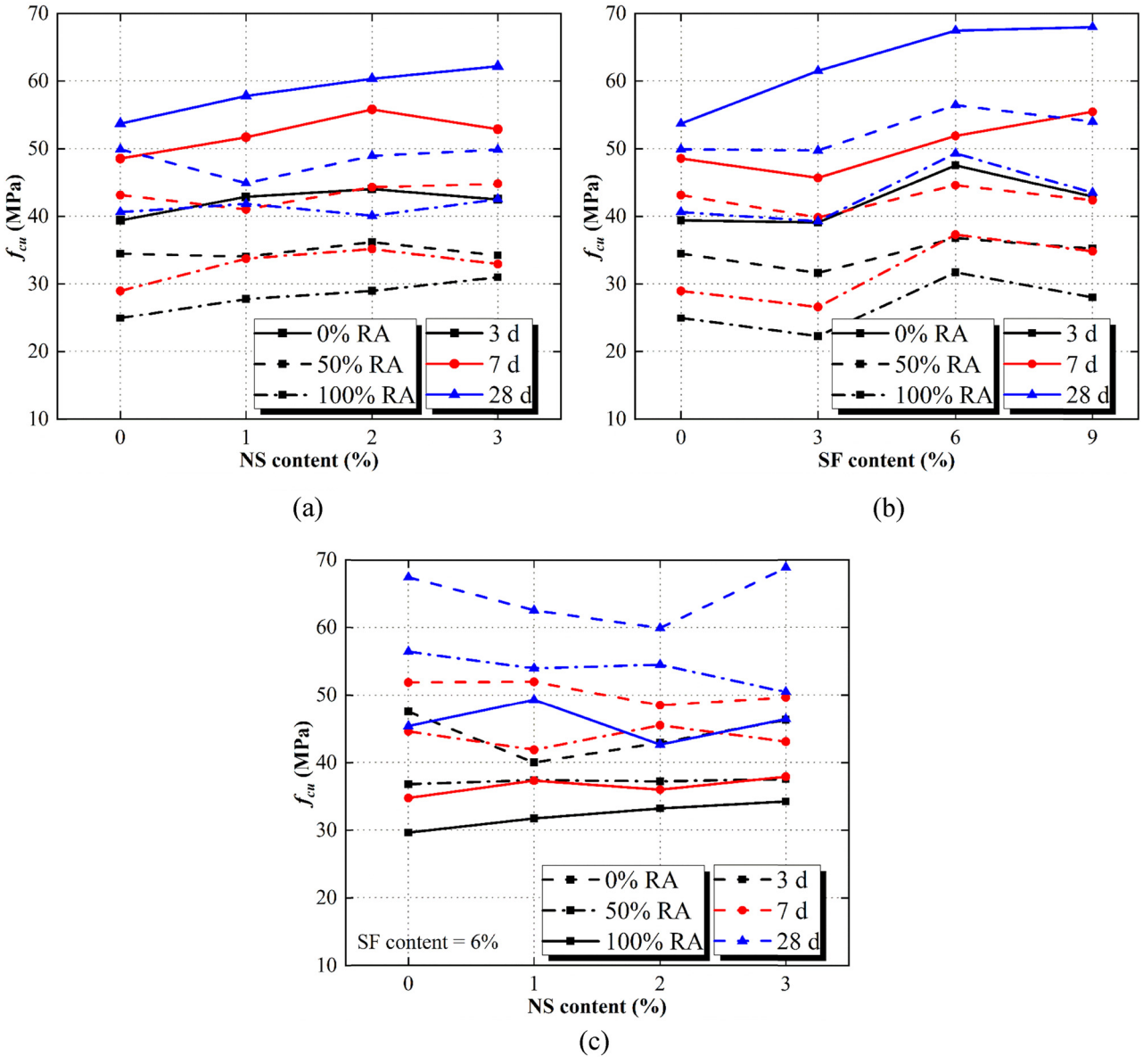

Figure 8: Effect of additives on the cubic compressive strength of concretes with (a) NS, (b) SF, and (c) NS and SF combined.

Table 7: Averaged growth rate of cubic compressive strength

Series	RA replacement (%)	Growth rate (3–7 days) (%)	Growth rate (7–28 days) (%)
Control group	0	23	11
	50	25	15
	100	16	20
NSRAC	0	24	13
	50	24	10
	100	16	22
SFRAC	0	18	29
	50	22	26
	100	20	34
SSRAC	0	17	28
	50	16	22
	100	12	24

50%, the f_{cu} of SSRAC did not significantly improve with the increase in NS content. When the RA replacement was 100%, the f_{cu} of SSRAC improved, particularly for the NS content of 3% at 3 days.

4.2.3 Effect of curing ages

As shown in Table 7, the growth rates of the three types of concrete in different ages showed that NS improved the strength of RAC, particularly the early strength (3 and 7 days). In contrast, with the use of SF, the growth rate of the strength of RAC was reduced at an early age and increased at a later age, which was consistent with the results of Cakir and Sofyanli [22]. The growth rate of SSRAC was uniform across all ages. As shown in Figure 9, when

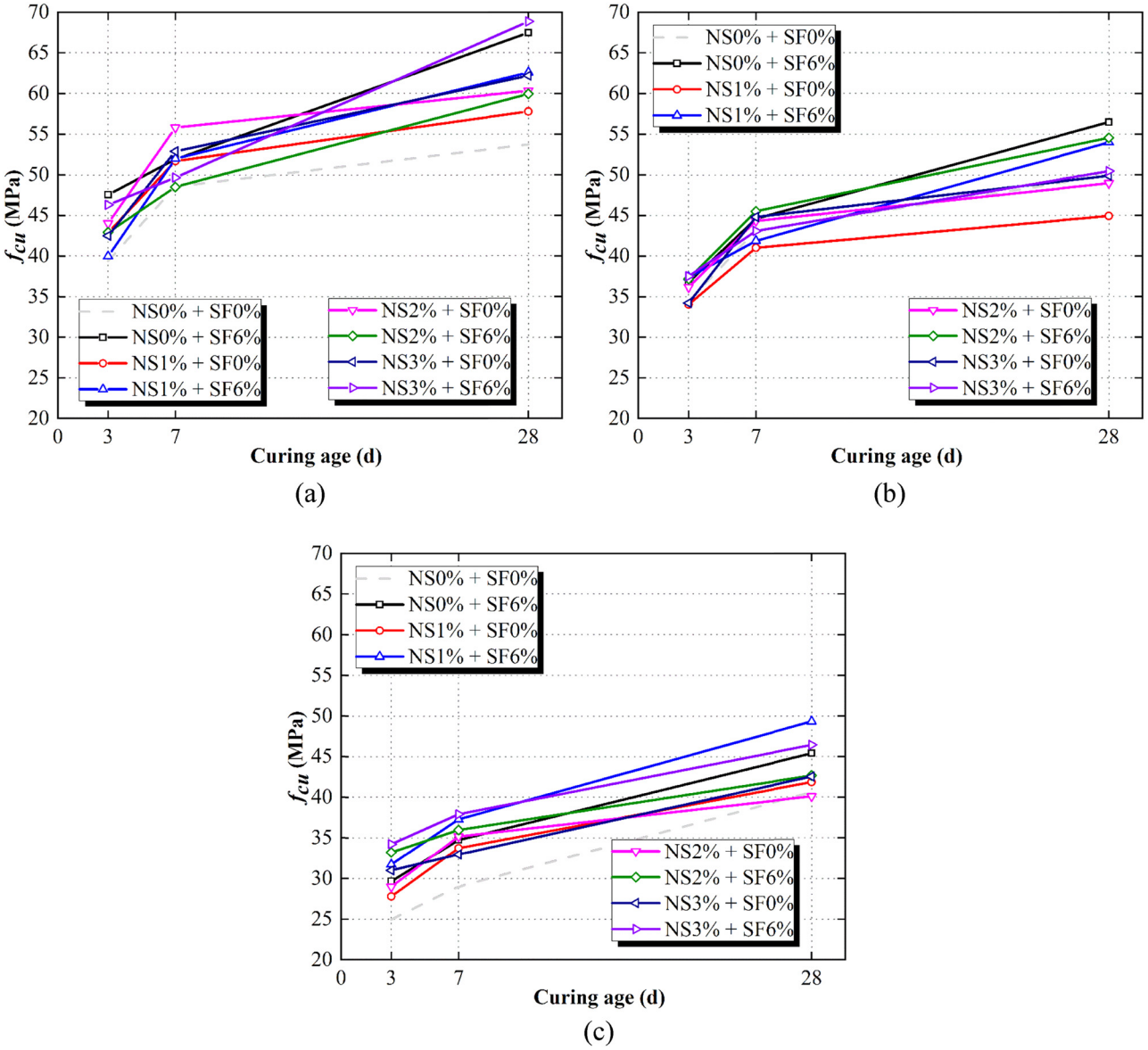

Figure 9: Effect of curing age on the cubic compressive strength of specimens with (a) 0%, (b) 50%, and (c) 100% RA replacement.

Table 8: Experimental results of split tensile strength

Specimen ID	f_t (MPa)		
	3 days	7 days	28 days
R0-NS0-SF0	3.63	3.61	3.40
R0-NS1-SF0	3.81	4.35	4.19
R0-NS2-SF0	4.27	4.75	4.44
R0-NS3-SF0	4.54	3.98	4.47
R50-NS0-SF0	2.68	3.19	3.50
R50-NS1-SF0	3.73	3.76	3.87
R50-NS2-SF0	3.49	3.43	3.67
R50-NS3-SF0	3.80	3.52	3.35
R100-NS0-SF0	2.63	2.92	2.91
R100-NS1-SF0	2.54	2.88	3.06
R100-NS2-SF0	2.61	3.15	3.57
R100-NS3-SF0	3.61	3.48	3.17
R0-NS0-SF6	3.60	4.89	4.33
R0-NS1-SF6	3.71	3.85	4.71
R0-NS2-SF6	4.19	4.73	4.89
R0-NS3-SF6	3.88	5.48	4.89
R50-NS0-SF6	3.09	4.24	4.08
R50-NS1-SF6	3.68	3.35	3.37
R50-NS2-SF6	3.54	3.88	4.15
R50-NS3-SF6	3.49	3.81	3.93
R100-NS0-SF6	2.80	3.47	3.39
R100-NS1-SF6	2.93	3.37	3.64
R100-NS2-SF6	2.91	3.43	3.38
R100-NS3-SF6	3.04	2.91	3.08

the RA replacement rate was 50%, the early compressive strengths of the three types of RAC were similar to that of the control group (without SF and NS), whereas the f_{cu} of SFRAC and SSRAC with SF were considerably improved at a later age. When the RA replacement rate was 100%, the compressive strength of SSRAC was the highest among the three age groups. According to the above results, it can be considered that when the RA replacement rate is more than 50%, it is recommended to combine NS and SF as SCMs for RAC.

4.3 Experimental results of split tensile strength

Because the previous section indicated that 6% is the optimal SF content, this content was selected to conduct the split tensile test. The experimental results of the tensile strength of RAC, NSRAC, SFRAC, and SSRAC are summarized in Table 8.

4.3.1 Failure modes

The fracture surfaces of specimens after the split tensile test are shown in Figure 10. Figure 10(a) shows the ITZ between the NA and the mortar without RA. Macroscopic observations showed that the interface was closely bonded. When the RA replacement was 50%, the internal structure was complex, exhibiting two ITZ types: one between the NA and mortar and one between the RA and mortar, as shown in Figure 10(b). For the RA replacement of 100% (Figure 10(c)), the internal structure was also complex, because RAs contained different types of materials and impurities with low strength (bricks, porcelains, *etc.*). In addition, harmful microcracks appeared in some RAs and weakened the properties of the ITZ.

4.3.2 Effect of RA replacement percentages

The relationship between f_t and the RA replacement percentages for NSRAC and SSRAC is plotted in Figure 11. With an increase in the RA replacement rate, the f_t of the NSRAC and SSRAC decreased. Similar to the cubic compressive strengths of NSRAC and SSRAC, the addition of NS and SF compensated for the strength loss caused by the incorporation of RA.

4.3.3 Effect of SCMs contents

As shown in Figure 12(a), the results indicated that when the RA replacement percentages were 0 and 100%, the f_t of NSRAC increased gradually with an increase in NS content, and the increase was more evident when the NS content was 2%. In contrast, for the RA replacement of 50%, there was no evident increase in f_t with an increase in NS. As shown in Figure 12(b), when the RA replacement rate was 0%, with the increase of NS content, the increase of f_t of SSRAC was evident. When the RA replacement percentages were 50 and 100%, the effects of adding NS and SF combined on SSRAC were minimal at later curing ages. This is because the promotion of the hydration reaction of cement by NS mainly occurs at early curing ages.

4.3.4 Effect of curing ages

Figure 13(a)–(c) show the effects of curing ages on f_t when the RA replacement percentages were 0, 50, and 100%,

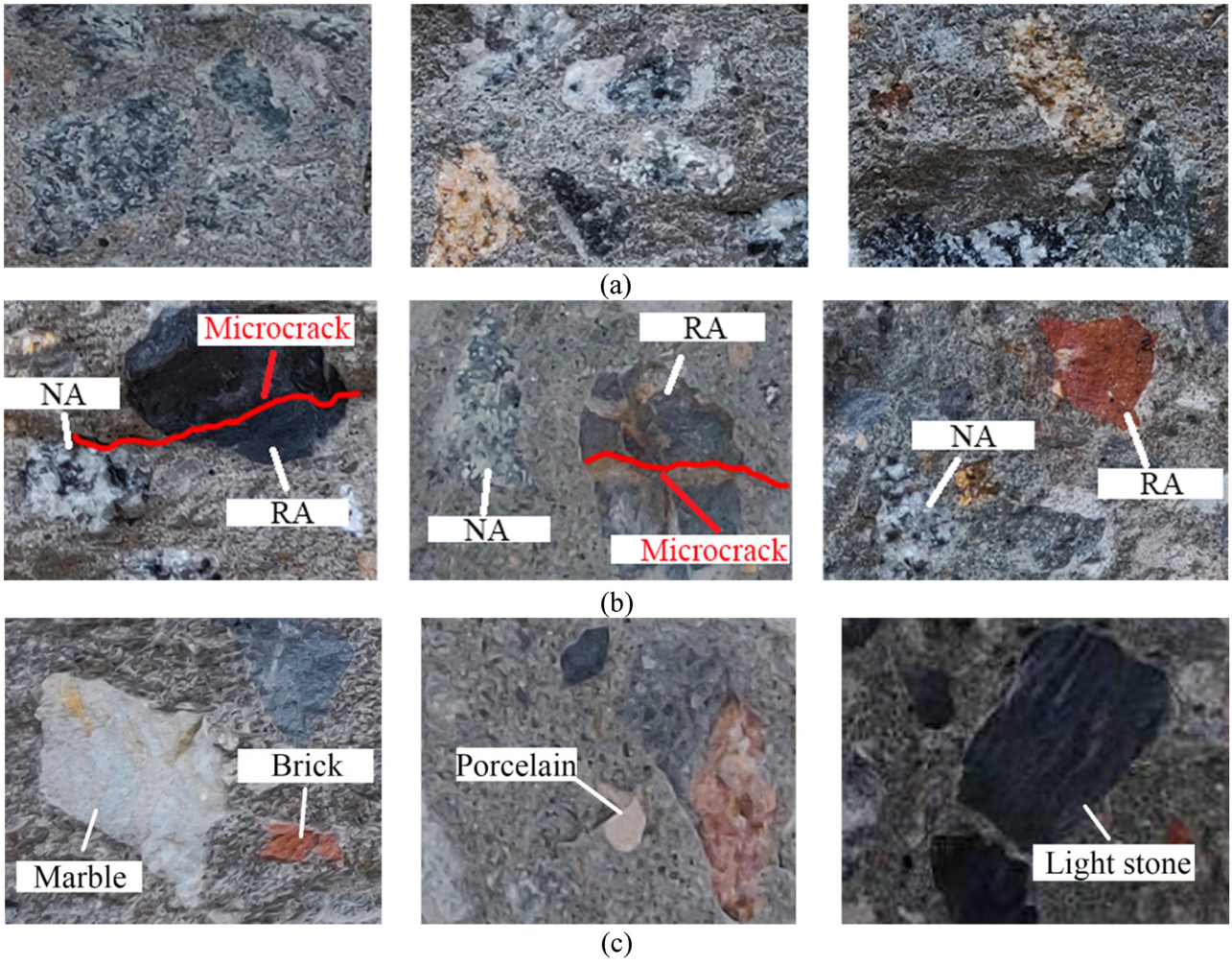

Figure 10: Failure modes of tensile test specimens: (a) 0%, (b) 50%, and (c) 100% RA replacement.

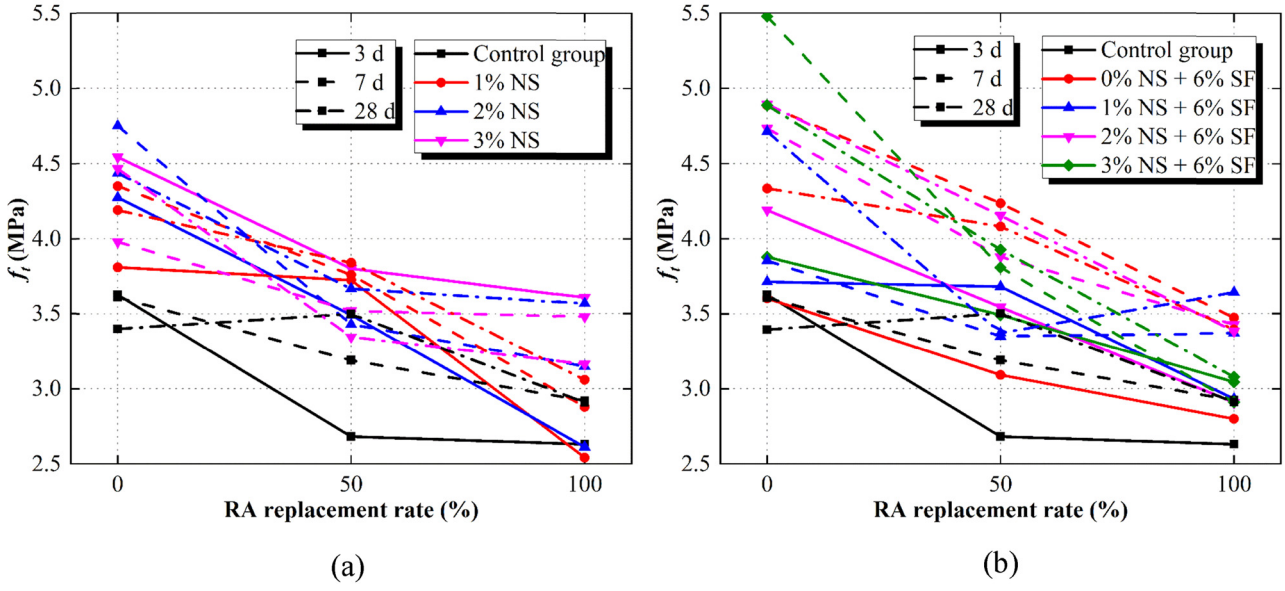

Figure 11: Effect of RA replacement percentage on the split tensile strength: (a) NSRAC and (b) SSRAC.

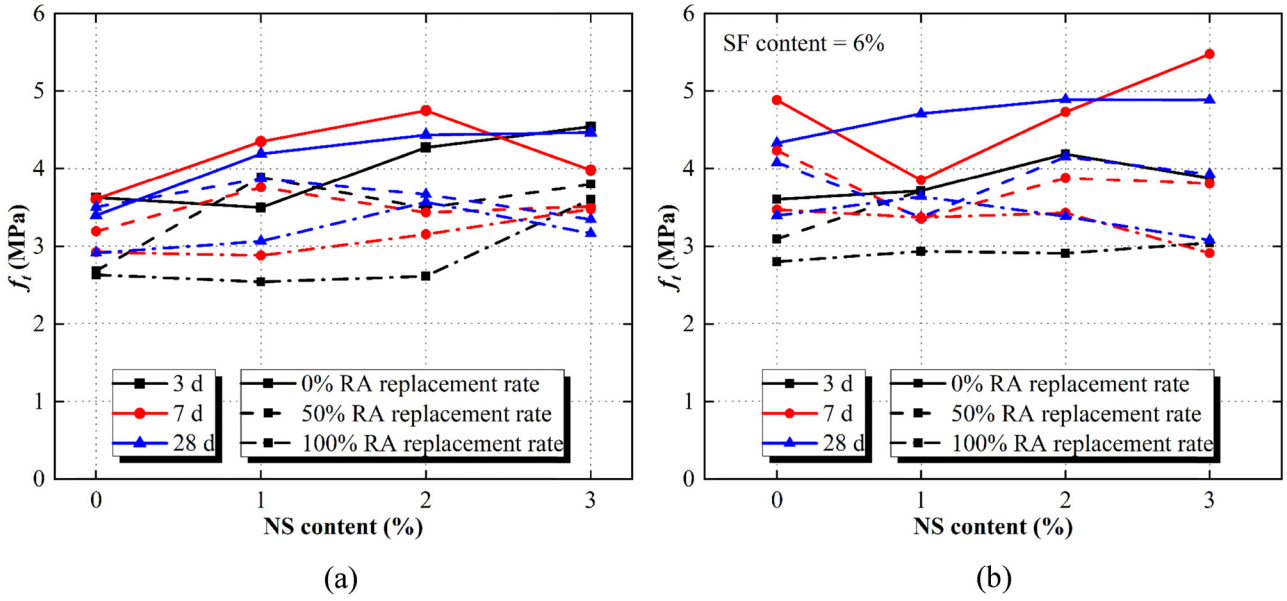

Figure 12: Effect of SCMs contents on the split tensile strength: (a) NSRAC and (b) SSRAC.

respectively. As shown in Figure 13(a), for 3 days, specimens with NS exhibited a considerable growth rate of f_t, whereas for 7 and 28 days, high growth rates of f_t were obtained for specimens with SF. Generally, the f_t of RAC at a later curing age was clearly improved by adding NS and SF in combination. As shown in Figure 13(b) and (c), when the curing age was 3 days, NS had a better promotion effect on f_t, whereas SF had a better promotion effect at 7 and 28 days. Therefore, when the RA replacement percentage is high, the NS content should also increase. Moreover, the addition of SF can improve the strength in later curing ages.

4.4 Experimental results of elastic properties

After the uniaxial compression test for SSRAC at 28 days, the experimental results of the stress–strain relationship, Young's modulus, and Poisson's ratio were obtained.

4.4.1 Failure modes

Figure 14 shows photographs of the typical failure modes. As shown in Figure 14(a) and (b), the specimens with 0% RA replacement exhibited several small microcracks and large inclined cracks, which are in agreement with the failure modes of ordinary concrete studied by Feng *et al.* [48]. In addition, the specimens with a 100% RA replacement exhibited evident concrete shedding at the extremities of the specimens. This was due to the defects of the RAs, which eased the crushing of the cylinders under a compressive load. However, as shown in Figure 14(c) and (d), the number of cracks on the surface of SFRAC and SSRAC was lower than that of RAC, and there were no evident large cracks. The surface of the specimens was relatively intact, which indicates that SF and NS could effectively inhibit the development of cracks when RAC was subjected to compressive loads.

4.4.2 Stress–strain relationship

As shown in Figure 15, when the RA replacement percentages were 0 and 50%, the peak strain of RAC slightly decreased with the addition of NS and SF. When the RA replacement was 100%, the peak strain of the RAC improved by adding NS and SF. Furthermore, for SSRAC with the same RA replacement percentage, the average peak strain remained almost unchanged with the increase in NS content. It can be considered that the NS content had no effect on the RAC with the same replacement percentage. In other words, the SF content was the main factor affecting peak strain.

4.4.3 Elastic properties

As shown in Figure 16(a), the Poisson's ratio of each group was approximately 0.2, which is similar to that of NAC. As shown in Figure 16(b), with an increase in the RA replacement percentage, the Young's modulus decreased. Compared with the specimens with 0% RA replacement,

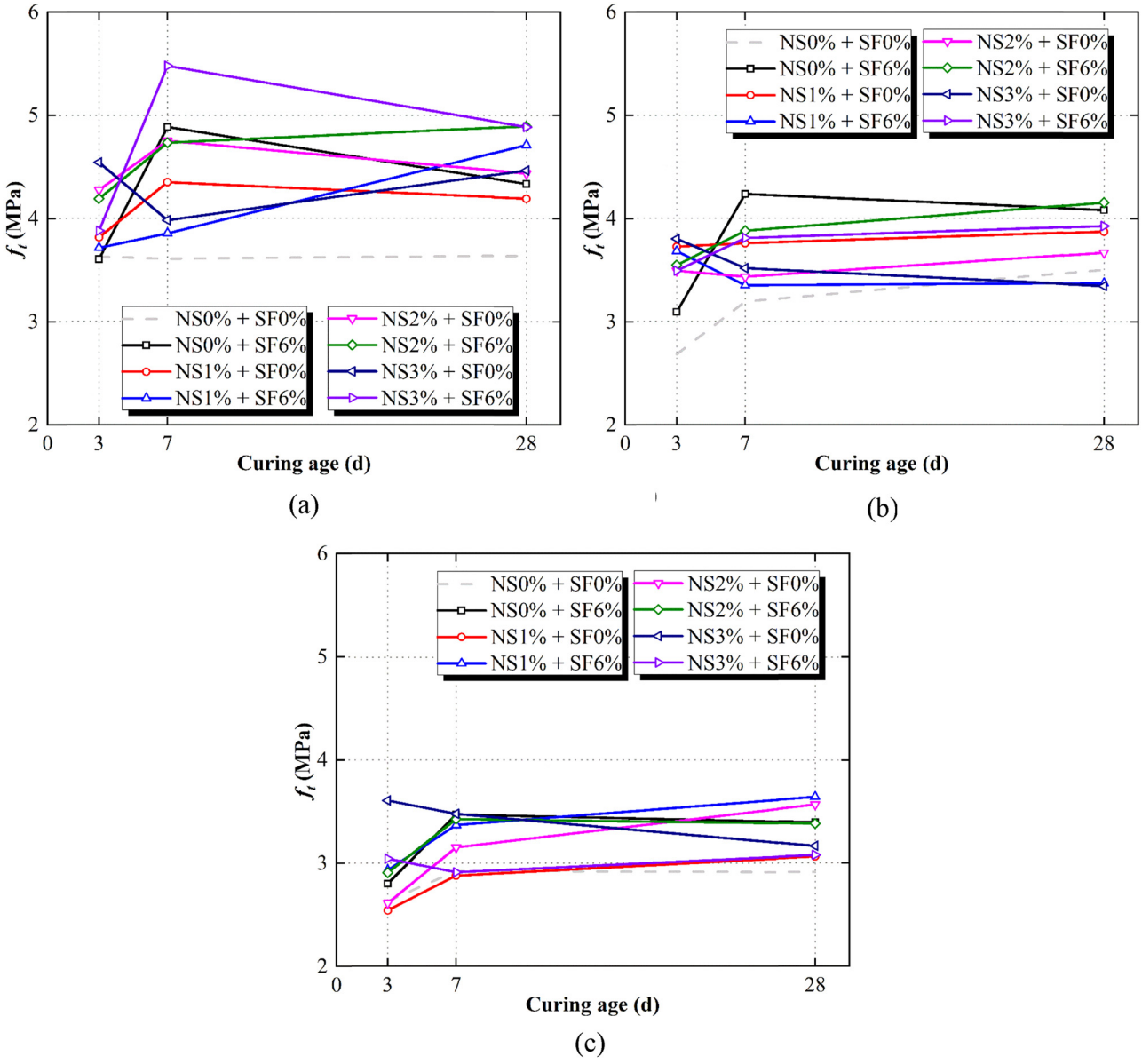

Figure 13: Effect of curing age on the split tensile strength of specimens with (a) 0%, (b) 50%, and (c) 100% RA replacement.

the Young's modulus with 50 and 100% RA replacement decreased by 21 and 43% on average, respectively. In addition, SF powders clearly increased the Young's modulus of RAC, but as the RA replacement percentage increased, this effect of SF gradually decreased. For the NS content, the change in the elastic modulus of SSRAC was small. Because of its pozzolanic characteristics, the addition of SF had a higher effect on the internal interface of concrete. On the one hand, SF participated in the pozzolanic reaction, densifying the microstructure of SSRAC. On the other hand, it filled the pores in concrete owing to its small size. Thus, the stiffness of the SSRAC was higher than that of the RAC.

5 Microstructure analysis

5.1 SEM micromorphology analysis

Some typical fragments of specimens after testing at 28 days were observed by SEM. As shown in Figure 17, the NS can fill the gap between the RA and mortar. The filling effect can be divided into physical and chemical filling. As NS microaggregated, it further enhanced the internal pore structure of the cement paste and improved the compactness of the RAC. In addition, NS, as an activator, accelerated the hydration of cement, changed the degree

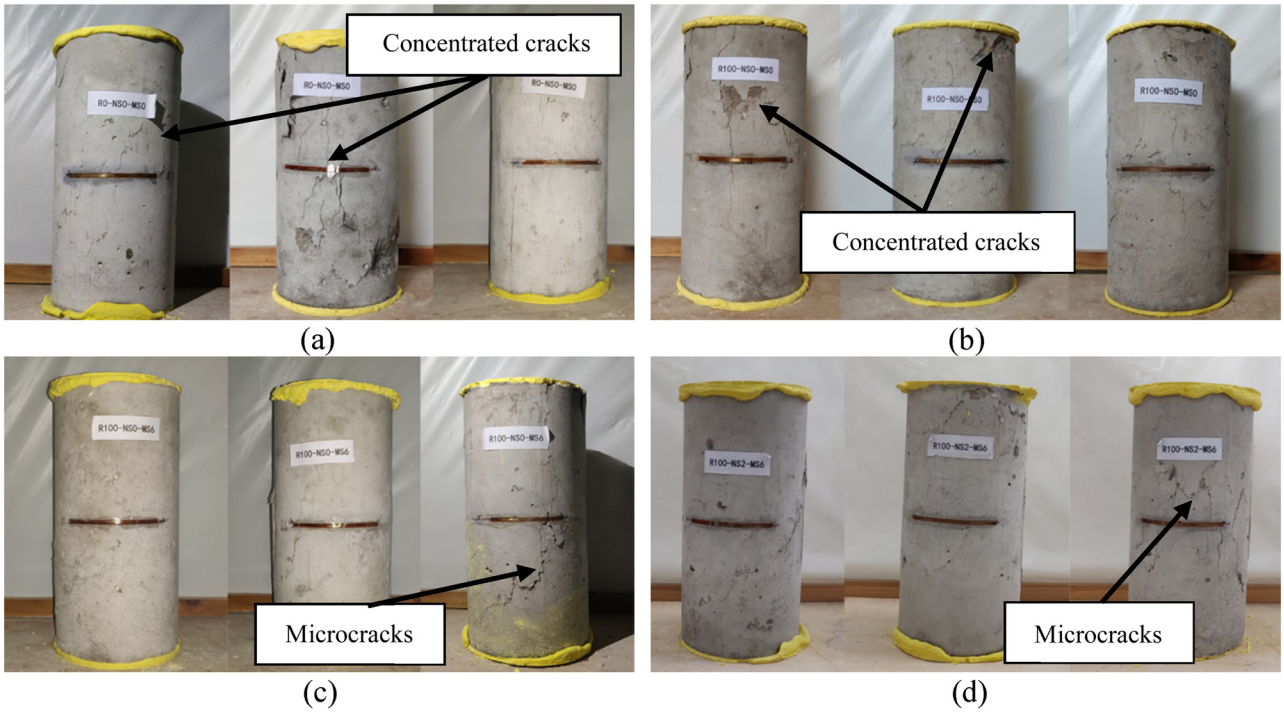

Figure 14: Typical failure modes of uniaxial compression test. (a) R0-NS0-SF0, (b) R100-NS0-SF0, (c) R100-NS0-SF6, and (d) R100-NS2-SF6.

of orientation of CH in the ITZ, and reacted with CH to form a low-density C–S–H gel, which filled the pores to make the internal structure dense. To further investigate the internal structure of NSRAC and SSRAC, a larger magnification (×8,000) was used to observe the microcracks, as shown in Figure 18, where the morphologies of CH and C–S–H were hexahedron plate-shaped and flocculent, respectively [49]. Because the particle size of NS was extremely small even with aggregation, only micropores were effectively filled. The structure of the remaining CH crystals was loose and porous, which had a negative effect on the internal structure of concrete. In contrast, SF particles were scattered in the cement paste, filling the internal voids. The generated C–S–H gel connected RA with mortar, and many ettringite crystals were observed filling the cracks. It can be considered that the combined use of NS and SF as SCMs can improve the microstructure of RAC and, consequently, its mechanical properties.

5.2 XRD phase analysis

XRD tests were conducted on RAC, SSRAC, and SFRAC specimens at the age of 28 days, and the diffraction patterns obtained are shown in Figure 19. As shown in Figure 19, the characteristic diffraction peak of silica for RAC (R100-NS0-SF0) was almost equal to that of NSRAC (R100-NS3-SF0), which indicates that the crystal structure of silica was stable. In addition, the characteristic diffraction peak of C–S–H was enhanced by adding NS and SF in combination. This phenomenon proved that both NS and SF had a good pozzolanic effect and underwent a secondary hydration reaction with CH to increase the production of C–S–H. Therefore, the characteristic diffraction peak of the CH of SSRAC was higher than that of NSRAC and RAC. In contrast, when only NS was used as SCM, the characteristic diffraction peak of C–S–H for SFRAC was close to that of RAC and significantly lower than that for SSRAC. This was one of the reasons for the lower strengths of NSRAC and RAC compared to that of SSRAC.

6 Conclusions

This study explored the mechanical properties and microstructure of RAC mixed with SF and NS (SSRAC); the following conclusions were drawn:

(1) NS and SF significantly reduced the fluidity of RAC. Thus, to be applied in engineering, the adoption of a water-reducing agent and high-speed mixing method to improve are suggested to improve the workability of SSRAC;

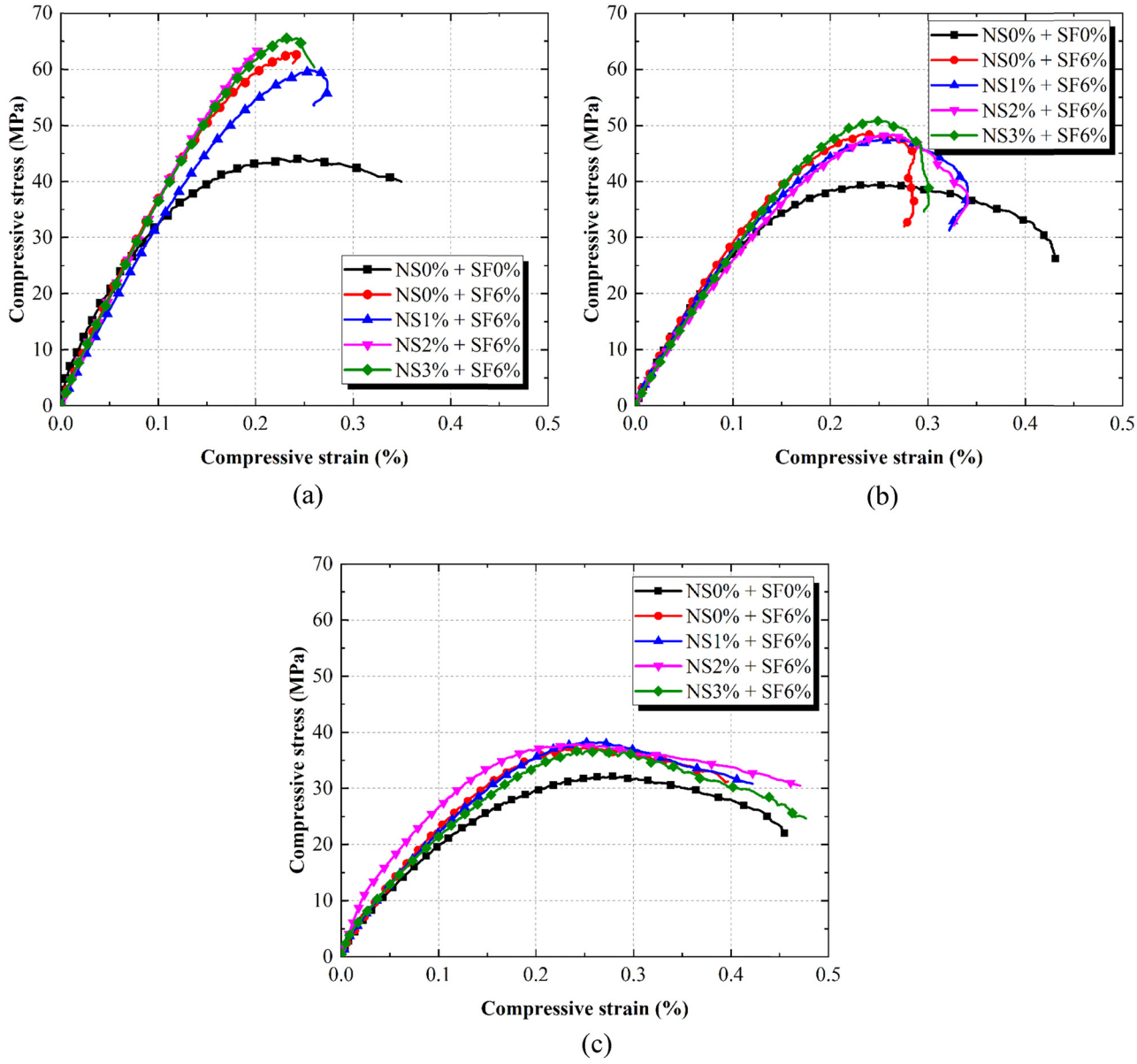

Figure 15: Stress–strain curves for specimens with different RA replacement percentages. (a) 0% RA, (b) 50% RA, and (c) 100% RA.

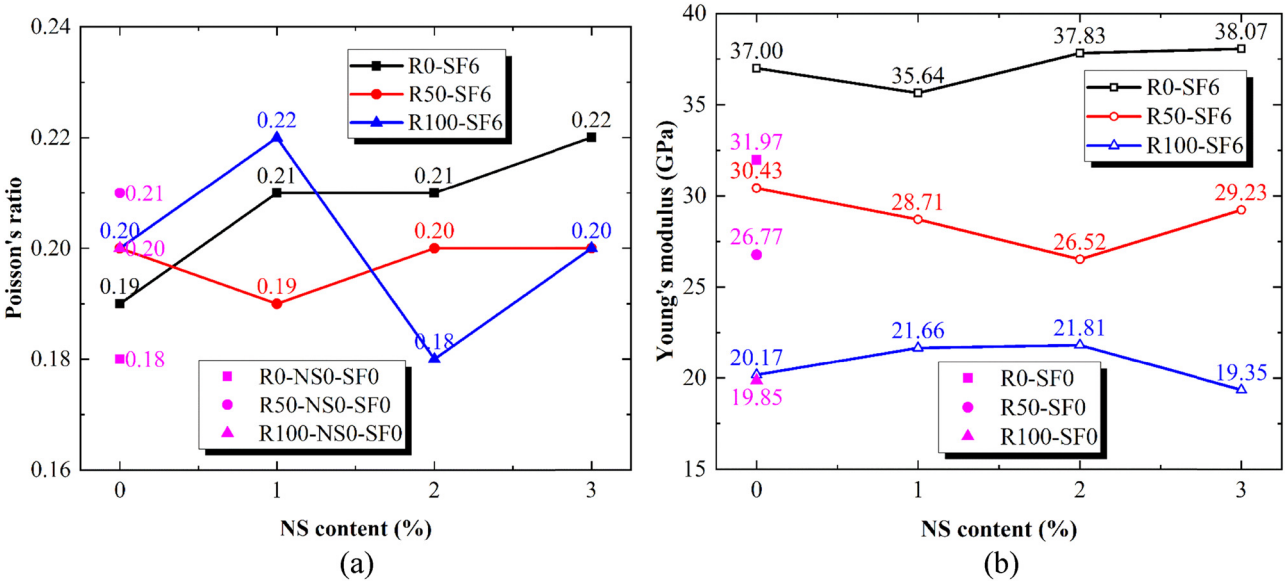

Figure 16: Experimental results of elastic properties: (a) Poisson's ratio and (b) Young's modulus.

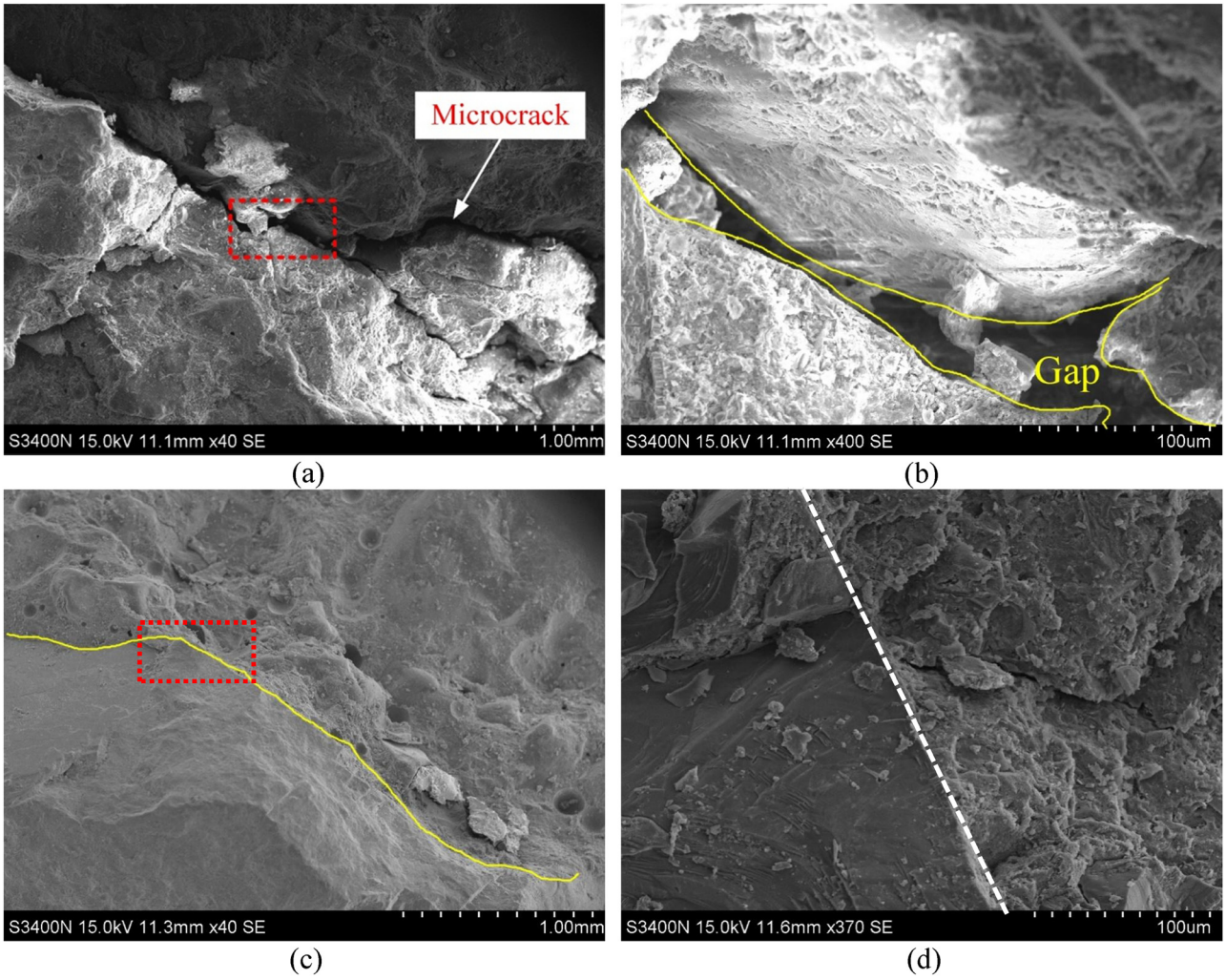

Figure 17: Comparison of microstructures of RAC and SSRAC. (a) RAC, (b) zoom in (a), (c) SSRAC, and (d) zoom in of (c).

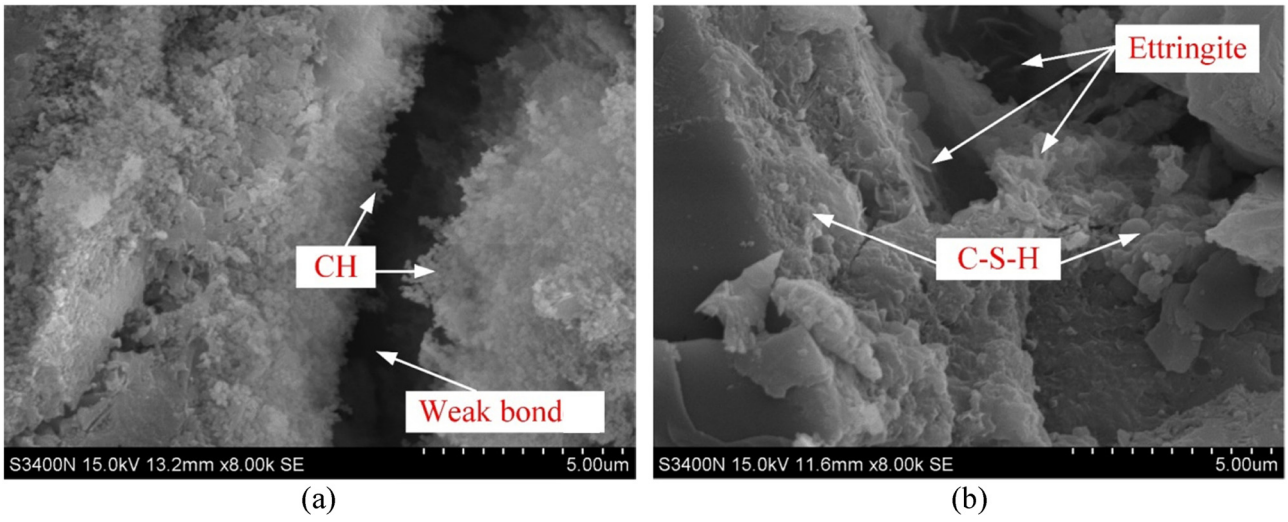

Figure 18: Comparison of microstructures of NSRAC and SSRAC. (a) NSRAC and (b) SSRAC.

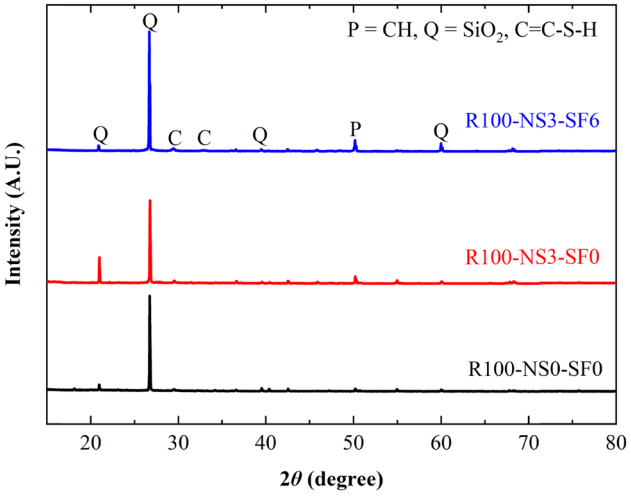

Figure 19: XRD patterns of RAC, SSRAC, and SFRAC.

(2) The use of RA reduced the compressive strength and splitting tensile strength of concrete. However, the addition of NS and SF resulted in improvements of these strengths of RAC, particularly at early and later ages, respectively;
(3) The elastic modulus of the RAC decreased with an increase in the RA replacement percentage. SF improved the elastic modulus of RAC, whereas NS had a slight effect. In addition, RA replacement percentage and SF and NS contents had no significant effect on Poisson's ratio, which was approximately 0.2 for all the combinations tested;
(4) NS and SF had a good pozzolanic effect and underwent a secondary hydration reaction with CH to increase the production of C–S–H. The products made the structure of the ITZ in SSRAC denser and inhibited the development of microcracks, thereby improving the loading capacity of the specimens.

Combining the characteristics of NS and SF, SSRAC exhibited good mechanical performance, and the percentages of 6% SF and 2 or 3% NS as SCMs are recommended. SSRAC can replace RAC in engineering applications for high-performance concrete structures.

7 Future research scopes

(1) There are limited data on the mechanical properties of SSRACs. One of our future works will be to summarize more experimental data to obtain a predicted model of strength at various curing ages with different RA replacement percentages and NS and SF contents;
(2) The durability of SSRAC will be studied to promote its utilization.

Funding information: This research was funded by the National Natural Science Foundation of China (Grant Nos. U2006224, 12032009, 51578162], China Postdoctoral Science Foundation (2021M690765), Special Funding Project of Guangdong Enterprise Science and Technology Commission (GDKTP2020029500), Key Field R&D Program Project of Guangdong Province, China (Grant No. 2019B020223003), and Guangxi Natural Science Foundation, China (GKAA18-242007, GKAA18118029).

Author contributions: All authors have accepted responsibility for the entire content of this manuscript and approved its submission.

Conflict of interest: The authors state no conflict of interest.

References

[1] Zhang W, Tang Z, Yang Y, Wei J, Stanislav P. Mixed-mode debonding behavior between CFRP plates and concrete under fatigue loading. J Struct Eng. 2021;147(5):04021055. doi: 10.1061/(ASCE)ST.1943-541X.0003032.
[2] Mou B, Bai Y. Experimental investigation on shear behavior of steel beam-to-CFST column connections with irregular panel zone. Eng Struct. 2018;168:487–504. doi: 10.1016/j.engstruct.2018.04.029.
[3] Huang H, Huang M, Zhang W, Pospisil S, Wu T. Experimental investigation on rehabilitation of corroded RC columns with BSP and HPFL under combined loadings. J Struct Eng. 2020;146(8):04020157. doi: 10.1061/(ASCE)ST.1943-541X.0002725.
[4] Iqbal MF, Javed MF, Rauf M, Azim I, Ashraf M, Yang J, et al. Sustainable utilization of foundry waste: forecasting mechanical properties of foundry sand based concrete using multi-expression programming. Sci Total Env. 2021;780:146524. doi: 10.1016/j.scitotenv.2021.146524.
[5] Zou R, Liu F, Xiong Z, He S, Li L, Wei W. Experimental study on fatigue bond behaviour between basalt fibre-reinforced polymer bars and recycled aggregate concrete. Constr Build Mater. 2021;270:121399. doi: 10.1016/j.conbuildmat.2020.121399.
[6] Iqbal MF, Liu Q, Azim I, Zhu X, Yang J, Javed MF, et al. Prediction of mechanical properties of green concrete incorporating waste foundry sand based on gene expression programming. J Hazard Mater. 2020;384:121322. doi: 10.1016/j.jhazmat.2019.121322.

[7] Xu Z, Huang Z, Liu C, Deng X, Hui D, Deng S. Research progress on mechanical properties of geopolymer recycled aggregate concrete. Rev Adv Mater Sci. 2021;60:158–72. doi: 10.1515/rams-2021-0021.
[8] Ahmed W, Lim CW. Production of sustainable and structural fiber reinforced recycled aggregate concrete with improved fracture properties: a review. J Clean Prod. 2021;279:123832. doi: 10.1016/j.jclepro.2020.123832.
[9] Hu Z, Mao L, Xia J, Liu J, Gao J, Yang J, et al. Five-phase modelling for effective diffusion coefficient of chlorides in recycled concrete. Mag Concr Res. 2018;70:583–94. doi: 10.1680/jmacr.17.00194.
[10] Xiong Z, Wei W, Liu F, Cui C, Li L, Zou R, et al. Bond behaviour of recycled aggregate concrete with basalt fibre-reinforced polymer bars. Compos Struct. 2021;256:113078. doi: 10.1016/j.compstruct.2020.113078.
[11] Tang YC, Fang S, Chen JM, Ma LY, Li LJ, Wu XG. Axial compression behavior of recycled-aggregate-concrete-filled GFRP–steel composite tube columns. Eng Struct. 2020;216:110676. doi: 10.1016/j.engstruct.2020.110676.
[12] Lee GC, Choi HB. Study on interfacial transition zone properties of recycled aggregate by micro-hardness test. Constr Build Mater. 2013;40:455–60. doi: 10.1016/j.conbuildmat.2012.09.114.
[13] Pradhan S, Kumar S, Barai SV. Multi-scale characterisation of recycled aggregate concrete and prediction of its performance. Cem Concr Compos. 2020;106:103480. doi: 10.1016/j.cemconcomp.2019.103480.
[14] Tang Y, Feng W, Chen Z, Nong Y, Yao M, Liu J. Experimental and theoretical investigation on the thermo-mechanical properties of recycled aggregate concrete containing recycled rubber. Front Mater. 2021;8:59. doi: 10.3389/fmats.2021.655097.
[15] Saravanakumar P, Abhiram K, Manoj B. Properties of treated recycled aggregates and its influence on concrete strength characteristics. Constr Build Mater. 2016;111:611–7. doi: 10.1016/j.conbuildmat.2016.02.064.
[16] Hosseini Zadeh A, Mamirov M, Kim S, Hu J. CO2-treatment of recycled concrete aggregates to improve mechanical and environmental properties for unbound applications. Constr Build Mater. 2021;275:122180. doi: 10.1016/j.conbuildmat.2020.122180.
[17] Khushnood RA, Qureshi ZA, Shaheen N, Ali S. Bio-mineralized self-healing recycled aggregate concrete for sustainable infrastructure. Sci Total Env. 2020;703:135007. doi: 10.1016/j.scitotenv.2019.135007.
[18] Yang Y, Chen Z, Feng W, Nong Y, Yao M, Tang Y. Shrinkage compensation design and mechanism of geopolymer pastes. Constr Build Mater. 2021;299:123916. doi: 10.1016/j.conbuildmat.2021.123916.
[19] Xu D, Liu Q, Qin Y, Chen B. Analytical approach for crack identification of glass fiber reinforced polymer–sea sand concrete composite structures based on strain dissipations. Struct Health Monit. 2020;1475921720974290. doi: 10.1177/1475921720974290.
[20] Hosan A, Shaikh FUA, Sarker P, Aslani F. Nano- and micro-scale characterisation of interfacial transition zone (ITZ) of high volume slag and slag-fly ash blended concretes containing nano SiO2 and nano CaCO3. Constr Build Mater. 2021;269:121311. doi: 10.1016/j.conbuildmat.2020.121311.
[21] Miraldo S, Lopes S, Pacheco-Torgal F, Lopes A. Advantages and shortcomings of the utilization of recycled wastes as aggregates in structural concretes. Constr Build Mater. 2021;298:123729. doi: 10.1016/j.conbuildmat.2021.123729.
[22] Çakır Ö, Sofyanlı ÖÖ. Influence of silica fume on mechanical and physical properties of recycled aggregate concrete. HBRC J. 2015;11:157–66. doi: 10.1016/j.hbrcj.2014.06.002.
[23] Wu Q, Miao WS, Zhang YD, Gao HJ, Hui D. Mechanical properties of nanomaterials: a review. Nanotechnol Rev. 2020;9:259–73. doi: 10.1515/ntrev-2020-0021.
[24] Lau D, Jian W, Yu Z, Hui D. Nano-engineering of construction materials using molecular dynamics simulations: Prospects and challenges. Compos Part B Eng. 2018;143:282–91. doi: 10.1016/j.compositesb.2018.01.014.
[25] Sun Y, Peng Y, Zhou T, Liu H, Gao P. Study of the mechanical-electrical-magnetic properties and the microstructure of three-layered cement-based absorbing boards. Rev Adv Mater Sci. 2020;59:160–9. doi: 10.1515/rams-2020-0014.
[26] Thompson L, Azadmanjiri J, Nikzad M, Sbarski I, Wang J, Yu A. Cellulose nanocrystals: production, functionalization and advanced applications. Rev Adv Mater Sci. 2019;58:1–16. doi: 10.1515/rams-2019-0001.
[27] Zhang H, Gao C, Li H, Pang F, Zou T, Wang H, et al. Analysis of functionally graded carbon nanotube-reinforced composite structures: a review. Nanotechnol Rev. 2020;9:1408–26. doi: 10.1515/ntrev-2020-0110.
[28] Feng P, Chang H, Liu X, Ye S, Shu X, Ran Q. The significance of dispersion of nano-SiO_2 on early age hydration of cement pastes. Mater Des. 2020;186:108320. doi: 10.1016/j.matdes.2019.108320.
[29] Fallah S, Nematzadeh M. Mechanical properties and durability of high-strength concrete containing macro-polymeric and polypropylene fibers with nano-silica and silica fume. Constr Build Mater. 2017;132:170–87. doi: 10.1016/j.conbuildmat.2016.11.100.
[30] Zareei SA, Ameri F, Bahrami N, Shoaei P, Moosaei HR, Salemi N. Performance of sustainable high strength concrete with basic oxygen steel-making (BOS) slag and nano-silica. J Build Eng. 2019;25:100791. doi: 10.1016/j.jobe.2019.100791.
[31] Yang H, Monasterio M, Zheng D, Cui H, Tang W, Bao X, et al. Effects of nano silica on the properties of cement-based materials: a comprehensive review. Constr Build Mater. 2021;282:122715. doi: 10.1016/j.conbuildmat.2021.122715.
[32] Ying J, Zhou B, Xiao J. Pore structure and chloride diffusivity of recycled aggregate concrete with nano-SiO2 and nano-TiO2. Constr Build Mater. 2017;150:49–55. doi: 10.1016/j.conbuildmat.2017.05.168.
[33] Zhang B, Tan H, Shen W, Xu G, Ma B, Ji X. Nano-silica and silica fume modified cement mortar used as surface protection material to enhance the impermeability. Cem Concr Compos. 2018;92:7–17. doi: 10.1016/j.cemconcomp.2018.05.012.
[34] Bernal J, Reyes E, Massana J, León N, Sánchez E. Fresh and mechanical behavior of a self-compacting concrete with additions of nano-silica, silica fume and ternary mixtures. Constr Build Mater. 2018;160:196–210. doi: 10.1016/j.conbuildmat.2017.11.048.
[35] Chinese Standard. GB175: Common Portland cement; 2007.
[36] Chinese Standard. JGJ 52: Standard for technical requirements and test method of sand and crushed stone (or gravel) for ordinary concrete; 2006.

[37] Chinese Standard. GB/T 25177: Recycled corase aggregate for concrete; 2010.
[38] Zare Y, Rhee KY, Hui D. Influences of nanoparticles aggregation/agglomeration on the interfacial/interphase and tensile properties of nanocomposites. Compos Part B Eng. 2017;122:41–6. doi: 10.1016/j.compositesb.2017.04.008.
[39] Chinese Standard. GB/T 50081: Standard for test methods of concrete physical and mechanical properties; 2019.
[40] ASTM-International. ASTM C469: standard test method for static modulus of elasticity and Poisson's ratio of concrete in compression; 2014.
[41] Sun J, Lin S, Zhang G, Sun Y, Zhang J, Chen C, et al. The effect of graphite and slag on electrical and mechanical properties of electrically conductive cementitious composites. Constr Build Mater. 2021;281:122606. doi: 10.1016/j.conbuildmat.2021.122606.
[42] Sun J, Huang Y, Aslani F, Wang X, Ma G. Mechanical enhancement for EMW-absorbing cementitious material using 3D concrete printing. J Build Eng. 2021;41:102763. doi: 10.1016/j.jobe.2021.102763.
[43] Li J, Qin Q, Sun J, Ma Y, Li Q. Mechanical and conductive performance of electrically conductive cementitious composite using graphite, steel slag, and GGBS. Struct Concr. 2020;1–15. doi: 10.1002/suco.202000617.
[44] Zhao R, Zhang L, Fan G, Chen Y, Huang G, Zhang H, et al. Probing the exact form and doping preference of magnesium in ordinary Portland cement clinker phases: A study from experiments and DFT simulations. Cem Concr Res. 2021;144:106420. doi: 10.1016/j.cemconres.2021.106420.
[45] Zhao N, Deng L, Luo D, Zhang P. One-step fabrication of biomass-derived hierarchically porous carbon/MnO nanosheets composites for symmetric hybrid supercapacitor. Appl Surf Sci. 2020;526:146696. doi: 10.1016/j.apsusc.2020.146696.
[46] Saba AM, Khan AH, Akhtar MN, Khan NA, Rahimian Koloor SS, Petrů M, et al. Strength and flexural behavior of steel fiber and silica fume incorporated self-compacting concrete. J Mater Res Technol. 2021;12:1380–90. doi: 10.1016/j.jmrt.2021.03.066.
[47] Xiao JZ, Wang CH, Ding T, Akbarnezhad A. A recycled aggregate concrete high-rise building: Structural performance and embodied carbon footprint. J Clean Prod. 2018;199:868–81. doi: 10.1016/j.jclepro.2018.07.210.
[48] Feng WH, Liu F, Yang F, Jing L, Li LJ, Li HZ, et al. Compressive behaviour and fragment size distribution model for failure mode prediction of rubber concrete under impact loads. Constr Build Mater. 2021;273:121767. doi: 10.1016/j.conbuildmat.2020.121767.
[49] Tang YC, Feng WH, Feng WX, Chen JM, Bao DJ, Li LJ. Compressive properties of rubber-modified recycled aggregate concrete subjected to elevated temperatures. Constr Build Mater. 2021;268:121181. doi: 10.1016/j.conbuildmat.2020.121181.